communications earth & environment

Article

A Nature Portfolio journal

https://doi.org/10.1038/s43247-025-02761-9

Calcium-rich parent materials enhance multiple soil functions and bacterial network complexity

Check for updates

Peilei Hu[1,2], Wei Zhang[1,2,7] ✉, Wolfgang Wanek[3], Ji Chen[4], Diego Abalos[5], Jie Zhao[1,2], Dan Xiao[1,2], Xinyu Hou[1,2,6], Juan Li[1,2,6], Hongsong Chen[1,2], Jun Xiao[1,2], Xionghui Liao[1,2], Tiangang Tang[1,2], Hanqing Wu[1,2] & Kelin Wang[1,2,7] ✉

Parent material shapes soil properties, yet its effects on soil functions and microbial networks remain unclear. Here we investigate these relationships using a large-scale field survey comparing soils derived from calcium-rich carbonate rocks and calcium-poor clastic rocks, complemented by a microcosm experiment. Soils from calcium-rich parent materials contained 33% higher organic carbon, 58% higher total nitrogen, and 55% higher total phosphorus than calcium-poor soils, yet lower labile carbon and several hydrolytic enzyme activities, with similar water retention. Calcium-rich soils exhibited greater bacterial network complexity, which associated with enhanced soil functions. Within calcium-rich soils, rock and soil calcium were primary drivers of increased carbon, nitrogen, and phosphorus storage and bacterial network complexity. The microcosm experiment confirmed that calcium-rich rock addition stimulated soil carbon and nitrogen cycling and enhanced bacterial network complexity, even in calcium-rich soils. These findings indicate calcium-rich parent materials can play a pivotal role in improving soil ecosystem services.

Soils play a pivotal role in sustaining ecosystem services by regulating the climate, biogeochemical cycles, and primary productivity[1]. As a result, maintaining soil functioning is crucial for sustainable development and human well-being[2]. Soil functions are inherently interconnected. Focusing on a single function in isolation risks skewing assessments of soil health and may inadvertently accelerate soil and environmental degradation[3]. Therefore, comprehensive research that assesses functionally distinct but interrelated processes—such as carbon, nitrogen, and phosphorus cycling, as well as water retention—is essential for advancing a mechanistic understanding of soil ecosystem services. While much research has emphasized plant or microbial diversity as key contributors to soil functions[1,4–6], the deeper, subsurface contributions of both the pedosphere and lithosphere have been largely overlooked.

Parent materials, forming the lower boundary of the critical zone, profoundly influence soil properties and functions. Rock weathering releases base cations and leads to the formation of short-range-order minerals[7], which are vital for stabilizing soil organic matter (SOM) through the formation of mineral-organic associations[8,9]. Variations in parent materials and their weathering rates create differences in the composition and saturation status of secondary minerals with high specific surface area, affecting SOM stabilization. These reactive minerals also enhance soil structure through aggregate stabilization, promoting water retention and nutrient storage[10]. Beyond phosphorus, which primarily originates from rock weathering[11,12], nitrogen released through rock weathering contributes 8–26% of the preindustrial terrestrial nitrogen balance, representing an important input to ecosystem nitrogen pools[13]. Despite these insights, the understanding of how parent materials simultaneously affect carbon, nitrogen, and phosphorus storage, as well as water retention, remains limited.

Parent materials also shape microbial communities by influencing soil attributes such as texture, pH, and nutrients[14,15]. Continuous rock weathering releases essential rock-derived elements, including phosphorus, nitrogen, calcium (Ca), and magnesium (Mg)[13,16], which alleviate microbial nutrient limitations and influence ecological network interactions[17]. For

[1]Institute of Subtropical Agriculture, Chinese Academy of Sciences, Changsha, China. [2]Huanjiang Agriculture Ecosystem Observation and Research Station of Guangxi, Guangxi Key Laboratory of Karst Ecological Processes and Services, Huanjiang Observation and Research Station for Karst Ecosystems, Chinese Academy of Sciences, Huanjiang, China. [3]Division of Terrestrial Ecosystem Research, Center of Microbiology and Environmental Systems Science, University of Vienna, Vienna, Austria. [4]State Key Laboratory of Loess and Quaternary Geology, Institute of Earth Environment, Chinese Academy of Sciences, Xi'an, China. [5]Department of Agroecology, Aarhus University, Tjele, Denmark. [6]University of Chinese Academy of Sciences, Beijing, China. [7]These authors jointly supervised this work: Wei Zhang, Kelin Wang. ✉e-mail: zhangw@isa.ac.cn; kelin@isa.ac.cn

example, soils derived from rocks rich in plant nutrients and carbonates exhibit greater bacterial network complexity compared to soils derived from rocks contain less of these elements[18]. Microbial network complexity is intricately linked to soil functioning[19]. Soil microorganisms form intricate networks resulting from a multitude of positive and negative, direct and indirect interactions[20,21]. The complexity of these networks, characterized not by species richness but by the associations among species[22], supports various soil functions, including carbon cycling[23], nutrient retention[22], and plant resilience[24]. Network complexity is often evaluated using co-occurrence network analyses[21], and its topological features provide insights into soil functions[25]. Yet, how parent materials shape microbial network complexity and its relationship to soil carbon, nitrogen, and phosphorus cycling remains an open question.

Ca-rich parent materials, including carbonate lithologies such as limestone and dolomite, as well as silicate lithologies like wollastonite, are widespread and exhibit diverse weathering rates. Carbonate parent materials, in particular, weather faster than other Ca-rich lithologies[26], potentially exerting a stronger influence on soil functions over short timescales. For instance, calcitic lime amendments have been shown to modify microbial communities and promote soil carbon sequestration[27]. Carbonate rock weathering also provides essential nutrients to soil microbes, enhancing the complexity of diazotrophic networks and supporting free-living nitrogen fixation[28]. Additionally, carbonates influence phosphorus cycling through abiotic processes, such as weathering, sorption, and precipitation, and biotic processes, including bioweathering and biomineralization, thereby increasing the complexity of phosphorus turnover[29]. Although these studies highlight specific soil function responses to Ca-rich carbonates, a comprehensive, mechanistic framework integrating parent materials, microbial networks, and concurrent carbon, nitrogen, and phosphorus cycling remains to be developed.

In this study, we conducted a large-scale field survey and a controlled microcosm experiment to assess the effect of Ca-rich parent materials on soil functions, including water retention, carbon cycling, nitrogen cycling, and phosphorus cycling (Fig. 1). In the field study, we compared 14 soil parameters and microbial network complexity between forest soils derived from carbonate (Ca-rich) and clastic (Ca-poor) parent materials across a broad climatic gradient. To further validate the effect of Ca-rich rock on soil carbon and nitrogen cycling and microbial network complexity in soils already have relatively high Ca content, we conducted a microcosm experiment by adding carbonate rock dust to soils derived from carbonate parent materials. We hypothesized that: (1) Ca-rich parent materials enhance soil carbon, nitrogen, and phosphorus storage, water retention, and bacterial network complexity compared to Ca-poor parent materials; (2) these enhanced functions primarily result from elevated rock and soil Ca levels; and (3) even in Ca-rich soils, Ca-rich rock addition further strengthen specific soil functions and microbial network complexity. Our findings provide observational and experimental evidence that Ca-rich parent materials promote soil carbon, nitrogen, and phosphorus storage and enhance bacterial network complexity, revealing an underappreciated mechanism by which they shape microbial interactions and soil ecosystem processes.

Results

Comparing soil functions between Ca-rich and Ca-poor parent materials

Soil functions differed between Ca-rich and Ca-poor parent materials (Fig. 2). Water retention, indicated by water holding capacity, was similar between the two soil types (Fig. 2a). Regarding carbon cycling, soils from Ca-rich parent materials had 33% higher soil organic carbon (SOC; $p < 0.05$, Fig. 2b) and 75% higher microbial biomass carbon ($p < 0.01$, Fig. 2c) compared to those from Ca-poor parent materials. However, dissolved organic carbon was 66% lower in Ca-rich parent materials ($p < 0.001$, Fig. 2d), and the activities of carbon-cycling enzymes, including β-D-glucosidase and β-xylosidase, were also lower ($p < 0.01$, Fig. 2f, g). For nitrogen cycling, soils from Ca-rich parent materials had 58% higher total nitrogen ($p < 0.01$, Fig. 2i) and greater activities of nitrogen-cycling enzymes, including β-N-acetyl-glucosaminidase and leucine amino peptidase ($p < 0.01$, Fig. 2k, l), while total inorganic nitrogen showed no significant difference (Fig. 2j). Regarding phosphorus cycling, total phosphorus content was 55% greater in soils from Ca-rich parent materials ($p < 0.05$, Fig. 2m), whereas the activity of the phosphorus-cycling enzyme (phosphatase) was lower ($p < 0.001$, Fig. 2n).

Comparing soil microbial network complexity between Ca-rich and Ca-poor parent materials

Soil microbial network complexity was visualized and analyzed using co-occurrence network analysis, which provides a potential mathematical

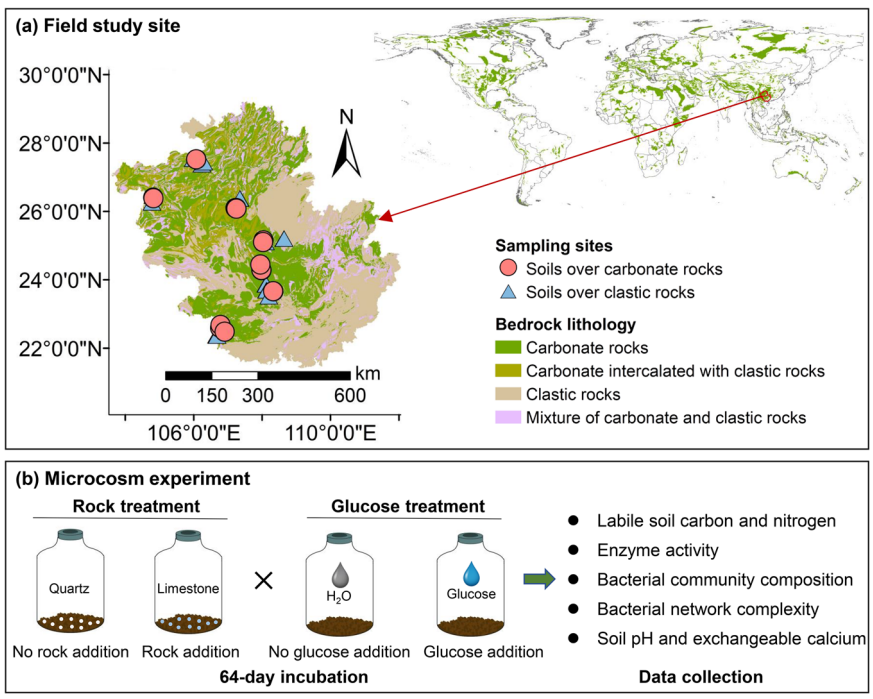

Fig. 1 | Overview of the field sampling sites and scheme of the microcosm experiment. **a** Geographic overview of the field sites overlying carbonate rocks (Ca-rich parent materials) and clastic rocks (Ca-rich parent materials). **b** Overview of the microcosm experimental design and data collection. Map lines delineate study areas and do not necessarily depict accepted national boundaries.

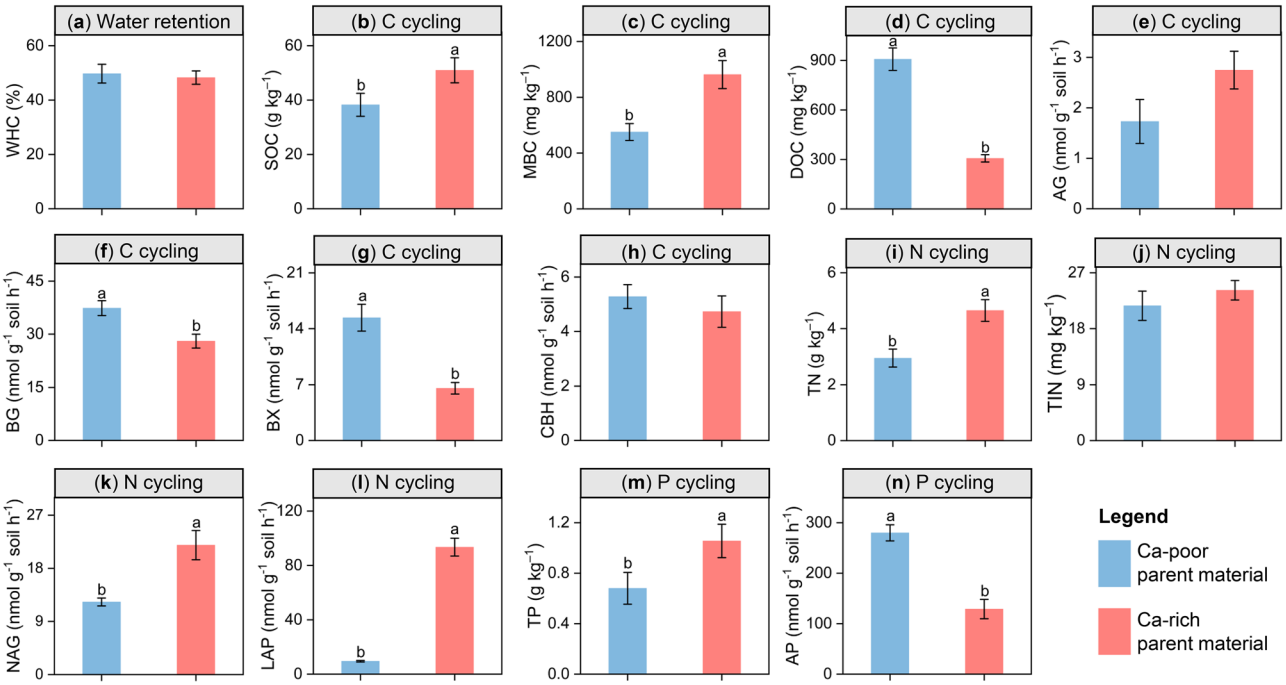

Fig. 2 | Soil parameters reflecting water retention, carbon cycling, nitrogen cycling, and phosphorus cycling in soils derived from Ca-rich and Ca-poor parent materials. a Soil water retention indicated by water holding capacity (WHC). Carbon (C) cycling parameters: soil organic carbon (SOC, **b**), microbial biomass carbon (MBC, **c**), dissolved organic carbon (DOC, **d**), α-glucosidase (AG, **e**), β-D-glucosidase (BG, **f**), β-xylosidase (BX, **g**), and β-D-cellobiosidase (CBH, **h**). Nitrogen (N) cycling parameters: total nitrogen (TN, **i**), total inorganic nitrogen (TIN, **j**), β-N-acetyl-glucosaminidase (NAG, **k**), and leucine amino peptidase (LAP, **l**). Phosphorus (P) cycling parameters: total phosphorus (TP, **m**) and acid or alkaline phosphorus (AP, **n**). Bars represent means ± standard errors ($n = 21$). Different lowercase letters represent significant differences at $p < 0.05$ between Ca-poor and Ca-rich parent materials.

framework to explore interactions within the microbial community. Soil microbial networks differed between Ca-rich and Ca-poor parent materials (Fig. 3). Both bacterial and fungal co-occurrence networks were more complex in Ca-rich parent materials (Fig. 3a, c). Topological analysis revealed that bacterial networks in Ca-rich soils had a higher average degree and increased numbers of edges and nodes compared to those in Ca-poor soils ($p < 0.01$, Fig. 3b). In fungal networks, the average degree was similar between the two soil types, yet numbers of edges and nodes were higher in soils derived from Ca-rich parent materials ($p < 0.01$, Fig. 3d).

Soil bacterial network complexity was closely associated with soil functions. In soils derived from Ca-rich parent materials, bacterial network complexity, particularly average degree and edge number, showed positive correlations with most soil functions, including water retention, multiple parameters of carbon and nitrogen cycling, and total phosphorus content (Supplementary Fig. 1a). For Ca-poor parent materials, bacterial network complexity, primarily average degree, showed positive correlations with soil water retention and the storage of carbon, nitrogen, and phosphorus (Supplementary Fig. 1b).

Dominant determinants of soil functions and microbial network complexity in Ca-rich and Ca-poor parent materials

Random forest analysis was employed to quantify the relative importance of multiple factors influencing soil functions and microbial network complexity, selected for its ability to rank variable importance in complex datasets. In Ca-rich soils, rock geochemistry (rock Ca and Ca/Mg ratio) and soil Ca (exchangeable Ca and Ca/Mg ratio) primarily affected most soil functions, showing positive correlations (Fig. 4a). In contrast, in Ca-poor soils, iron (hydr)oxides and bacterial abundance were the primary determinants of soil functions, also with positive correlations (Fig. 4b).

For microbial network complexity, distinct patterns emerged. In Ca-rich soils, soil Ca (e.g., exchangeable Ca and $CaCO_3$) predominantly influenced bacterial network complexity, exhibiting positive correlations (Supplementary Fig. 2a). Fungal network complexity in these soils was affected by climate, soil exchangeable Mg, pH, and fungal diversity, all positively correlated (Supplementary Fig. 2a). Conversely, in Ca-poor soils, climate was the dominant factor for both bacterial and fungal network complexity, showing negative effects (Supplementary Fig. 2b).

Notably, these influencing factors differed between Ca-rich and Ca-poor parent materials (Supplementary Table 1). Ca-rich soils had higher Ca (exchangeable Ca, $CaCO_3$, CaO), Mg (exchangeable Mg, MgO), and Ca/Mg ratio compared to Ca-poor soils. Additionally, Ca-rich soils had greater bacterial abundance and diversity but lower fungal abundance with higher diversity than Ca-poor soils.

Mechanistic drivers of Ca-rich parent materials on soil functions and bacterial network complexity based on field statistical analysis

The single-function approach revealed that rock and soil Ca content, along with Ca/Mg ratio, positively influenced specific soil functions in soils from Ca-rich parent materials (Fig. 4a). However, this approach did not capture the integrated performance of soil functions. The multiple-threshold approach assessed the concurrent performance of multiple soil functions, showing a positive correlation with rock and soil Ca content and Ca/Mg ratio (Fig. 5). Bacterial network complexity within Ca-rich parent materials was also positively associated with rock and soil Ca content and Ca/Mg ratio (Fig. 6), whereas fungal network complexity showed no such association (Supplementary Fig. 3). These results indicate that higher Ca levels within Ca-rich parent materials enhances multiple soil functions and bacterial network complexity.

Mechanistic drivers of Ca-rich parent materials on soil functions and bacterial network complexity based on experimental microcosm analysis

In the microcosm experiment, we evaluated the effects of adding limestone powder (Ca-rich rock) to karst soils (Ca-rich soil) on carbon and nitrogen

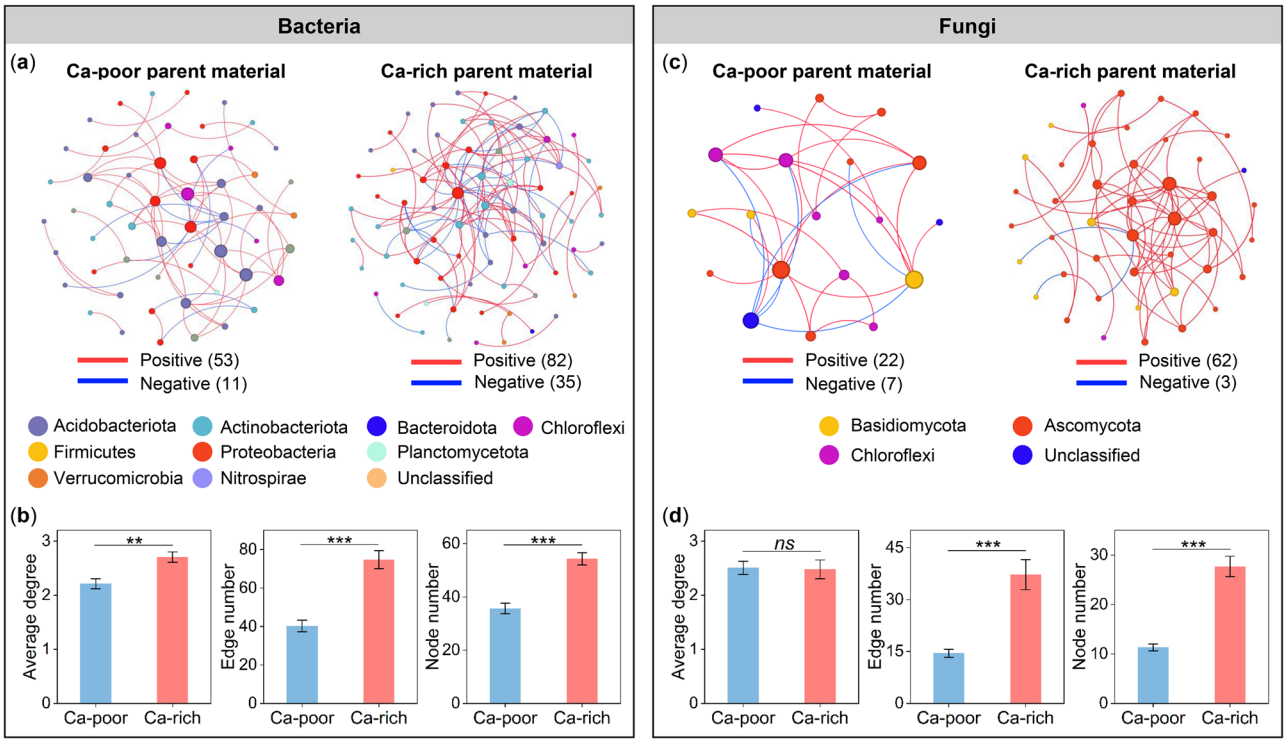

Fig. 3 | Microbial network complexity in soils derived from Ca-rich and Ca-poor parent materials. a, **c** Co-occurrence networks of soil bacterial and fungal communities. The sizes of the nodes (OTUs) are proportional to the number of connections. Only nodes that were significantly correlated with each other ($p < 0.05$) were connected (edges). **b**, **d** Bacterial and fungal network topological characteristics, including average degree, edge number, and node number. Bars in (**b**) and (**d**) represent means ± standard errors. $^{**}p < 0.01$; $^{***}p < 0.001$. ns not significant ($p > 0.05$).

cycling and bacterial network complexity over 64 days. Soil dissolved organic carbon and nitrogen were similar between treatments (Fig. 7a). In contrast, the activities of nitrogen-cycling enzyme (leucine amino peptidase) and carbon-cycling enzymes (polyphenol oxidase and peroxidase) were significantly elevated in the rock addition treatment compared to the control (Fig. 7a). Without external labile carbon (glucose) inputs, rock addition increased the activities of polyphenol oxidase and peroxidase by 100% and 68%, respectively, relative to the control. With glucose, these increases were 52% and 44%, respectively. Soil pH and exchangeable Ca also increased in the rock addition treatment ($p < 0.01$, Fig. 7b). Additionally, rock addition enhanced bacterial co-occurrence network complexity (Fig. 7c), with higher node and edge numbers, greater average degree, shorter path lengths, smaller diameter, and lower betweenness (Fig. 7d).

Discussion

Our field survey showed that soils derived from Ca-rich parent materials stored 33% more SOC, 58% more total nitrogen, and 55% more total phosphorus than Ca-poor soils (Fig. 2). However, labile soil carbon, measured as dissolved organic carbon, and the activities of hydrolytic enzymes involved in carbon-cycling, such as β-D-glucosidase and β-xylosidase, were lower in Ca-rich soils (Fig. 2). Within these Ca-rich soils, elevated levels of rock and soil Ca, including Ca content and the Ca/Mg ratio, emerged as the primary drivers enhancing carbon, nitrogen, and phosphorus storage (Figs. 4a and 5). These findings align with our hypothesis, confirming that Ca-rich parent materials foster the accumulation of total carbon, nitrogen, and phosphorus in soils.

Soils originating from Ca-rich parent materials typically have higher SOC content. First, soil Ca boosts microbial carbon use efficiency, increasing the incorporation of plant litter into microbial biomass and byproducts, thus promoting microbial-derived carbon accumulation[30]. Second, Ca enhances SOC stability by facilitating the association of microbial products and plant compounds with soil minerals[31,32]. Consistent with these mechanisms, both SOC and mineral-associated organic carbon increased with exchangeable Ca and $CaCO_3$ in Ca-rich soils (Supplementary Fig. 4). The lower dissolved organic carbon content in these soils, relative to Ca-poor soils, stems from the role of Ca in stabilizing SOC, which reduces labile carbon availability[33]. Consequently, limited labile carbon suppresses the activities of hydrolytic enzymes like β-D-glucosidase and β-xylosidase[34].

The increased storage of nitrogen and phosphorus in soils derived from Ca-rich parent materials, compared to those from Ca-poor parent materials, arises from two key mechanisms. First, carbonate rocks often contain phosphorus in the form of apatite [$Ca_{10}(PO_4)_6(OH,F,Cl)_2$][12] and nitrogen from sedimentary formations[13]. Although carbonate rocks may have lower absolute contents of nitrogen and phosphorus than clastic rocks[12,35], they weather over ten times faster[26]. Consequently, this rapid weathering releases greater amounts of rock-derived nitrogen and phosphorus during initial pedogenesis than does clastic rock weathering. Second, high soil Ca content from Ca-rich parent materials enhance nitrogen and phosphorus retention through adsorption and occlusion by Ca ion and $CaCO_3$. In contrast, lower phosphatase activity in these soils, compared to Ca-poor soils, reflects the role of Ca in promoting strong phosphorus sorption and precipitation. This process sequesters a large, poorly bioavailable phosphorus pool[36], suppressing microbial phosphatase production and decreasing enzyme activity. Additionally, the neutral to slightly alkaline conditions in Ca-rich soils may limit alkaline phosphatase activity relative to acid phosphatase in acidic, Ca-poor soils[37]. Together, these mechanisms explain why soils from Ca-rich parent materials accumulate larger total nitrogen and phosphorus pools yet exhibit reduced phosphatase activity.

Although Ca-rich parent materials increased carbon, nitrogen, and phosphorus storage, soil water retention did not differ between the two soil types (Fig. 2a), contrary to our hypothesis. This suggests that factors beyond soil Ca influence water retention. In Ca-rich sites, high Ca content promotes soil particle aggregation, forming porous structures with improved aeration[38], which bolsters water retention. The random forest analysis identified $CaCO_3$

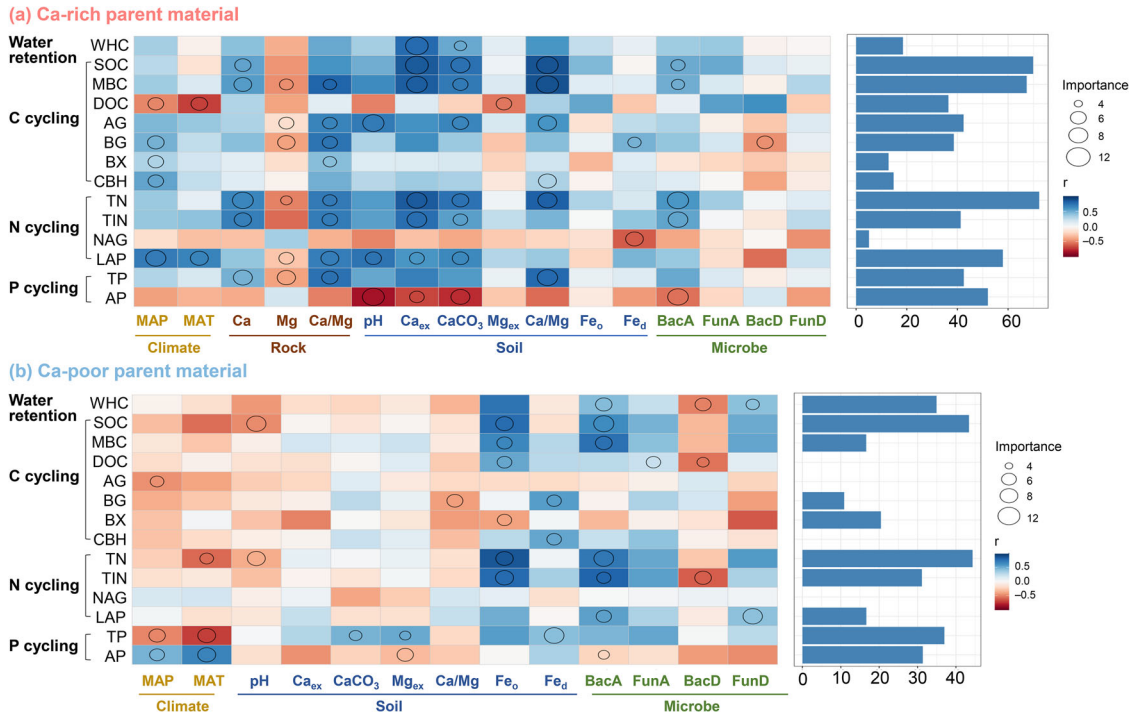

Fig. 4 | Relative importance of climate, rock geochemistry, soil pH and minerals, and microbial properties in explaining soil function variation. a Contributions of these factors to soil functions and their relationships in soils derived from Ca-rich parent materials. **b** Contributions of these factors to soil functions and their relationships in soils derived from Ca-poor parent materials. The effect of rock geochemistry on soil functions in Ca-poor parent materials was not evaluated due to the inaccessibility of these rocks. Circles within boxes indicate predictors that significantly explain the variation in corresponding soil functions at $p < 0.05$ level, as determined by random forest analysis; the size of each circle reflects the predictor's explanatory power. Predictor importance was assessed using the permutation-based increase in mean squared error (%IncMSE) over 100 permutations of the response variable. Box colors represent the correlation between predictors and soil functions based on Pearson's correlation coefficients, with a color gradient ranging from blue (positive) to red (negative). The combined use of random forest and Pearson's correlation analyses enables the assessment of both the significance and direction of each predictor's influence on soil functions. WHC water holding capacity, SOC soil organic carbon, MBC microbial biomass carbon, DOC dissolved organic carbon, AG α-glucosidase, BG β-D-glucosidase, BX β-xylosidase, CBH β-D-cellobiosidase, TN total nitrogen, TIN total inorganic nitrogen, NAG β-N-acetyl-glucosaminidase, LAP leucine amino peptidase, TP total phosphorus, AP acid or alkaline phosphatase, MAP mean annual precipitation, MAT mean annual temperature, Ca total calcium, Mg total magnesium, Ca/Mg ratio of total calcium to magnesium, Ca_{ex} exchangeable calcium, $CaCO_3$ calcium carbonate, Mg_{ex} exchangeable magnesium, Fe_o amorphous iron (hydr)oxides, Fe_d pedogenic iron (hydr)oxides, BacA bacterial abundance, FunA fungal abundance, BacD bacterial Shannon diversity, FunD fungal Shannon diversity.

as a key predictor of water retention within Ca-rich soils (Fig. 4a). In contrast, Ca-poor sites had higher above- and below-ground plant biomass carbon densities (Supplementary Fig. 5). Elevated plant biomass likely enhances soil water retention by improving physical structure and organic matter content[39]. These findings demonstrate that while plant productivity regulates soil water retention, Ca-rich parent materials can sustain comparable water retention even in ecosystems with lower plant productivity.

Consistent with our hypothesis, the field survey demonstrated that Ca-rich parent materials enhanced soil microbial network complexity, particularly for bacterial networks, compared to Ca-poor parent materials (Fig. 3). Three mechanisms likely contribute to this phenomenon. First, Ca-rich soils stored higher contents of carbon, nitrogen, and phosphorus (Fig. 2). These nutrient-enriched soils support more diverse and highly connected microbial networks, as abundant resources promote niche differentiation and interspecies interactions[40]. Consistent with the mechanism, bacterial network complexity (indicated by average degree) was positively associated with soil carbon, nitrogen, and phosphorus contents both in Ca-rich and Ca-poor parent materials (Supplementary Fig. 1). Second, the dissolution of Ca-rich parent materials releases and accumulates Ca in the soil (Supplementary Fig. 6). High Ca levels stabilize bacterial cell membranes, promoting cell division, gene expression, and differentiation[41]. Additionally, Ca-bearing minerals provide physicochemical protection and serve as bio-essential elements for microbes[42]. These processes foster bacterial interspecies interactions, amplifying bacterial network complexity in Ca-rich soils[43]. Notably, soil Ca had little influence on microbial network topology in Ca-poor soils (Supplementary Fig. 2b), where baseline Ca content are low and small Ca fluctuations likely exert minimal impact. Third, soils from Ca-rich parent materials typically maintain neutral to slightly alkaline pH (Supplementary Table 1). This pH range favors diverse bacterial groups, enhancing overall bacterial network complexity[44]. Together, high nutrient storage, elevated Ca, and optimal pH in Ca-rich soils synergistically strengthen microbial interspecies interactions, particularly among bacteria.

Bacterial network complexity was positively associated with most soil functions (Supplementary Fig. 1). Although these correlations do not imply causation, they underscore the value of considering bacterial networks in promoting soil multifunctionality. Generally, greater storage of SOM and associated nutrients tend to support more intricate bacterial networks[40]. In turn, complex networks foster positive microbial interactions, such as niche differentiation or mutual facilitation, which enhance soil functioning[25]. For instance, greater microbial network complexity correlates with higher efficiency in soil carbon and nutrient cycling[45]. We observed that higher bacterial network complexity was positively correlated with increased microbial carbon use efficiency in soils derived from Ca-rich parent materials (Supplementary Fig. 7). Moreover, negative interactions within complex networks, such as competition, can stabilize microbial co-oscillations, promoting community resilience and functional stability[46]. This stability enhances microbial resistance to environmental stress, potentially supporting processes like carbon cycling[23] and soil enzyme activity[47]. Consequently, bacterial

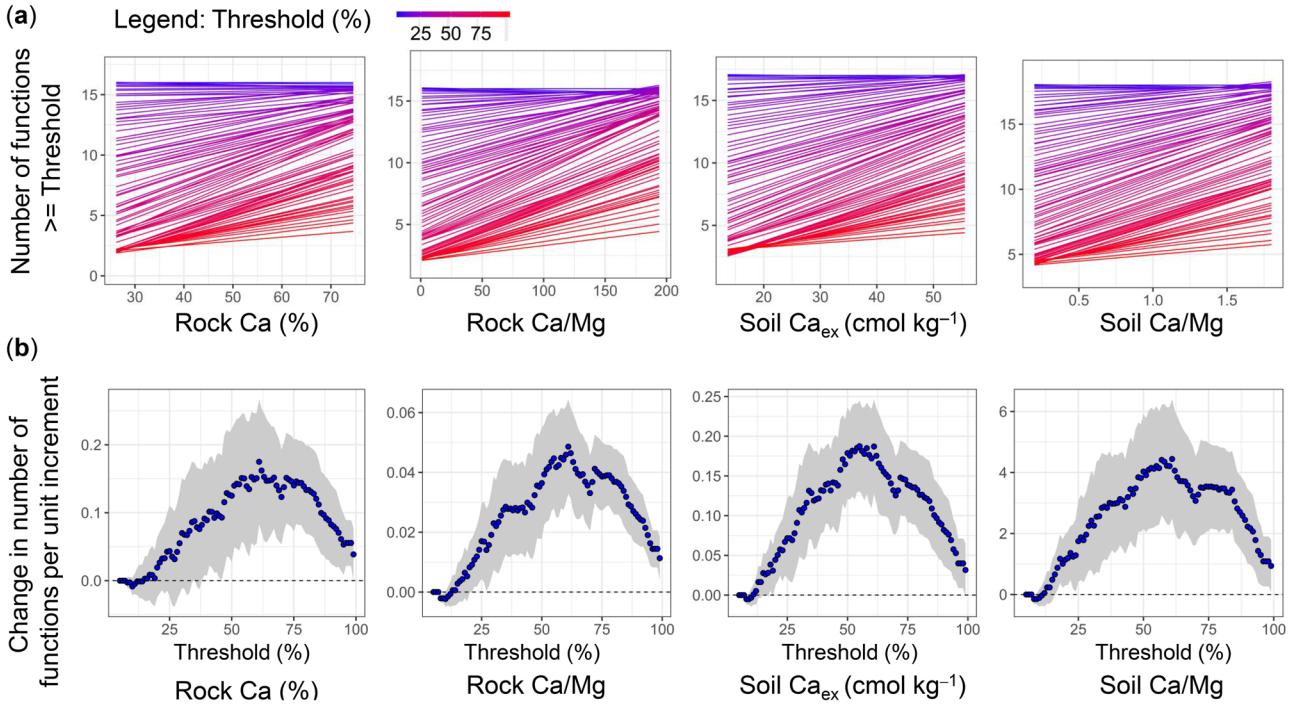

Fig. 5 | Effects of rock and soil Ca on multiple soil functions within Ca-rich parent materials. a Regressions between the number of soil functions exceeding a given threshold and rock or soil Ca. Thresholds were defined as percentages (5–99% at 1% increments) of each function's maximum observed value (calculated as the mean of the top four measurements). Colors represent different threshold levels, with cooler colors indicating lower thresholds and warmer colors indicating higher thresholds, as detailed in the figure legend. **b** Slope of the relationship between the number of soil functions exceeding a given threshold and rock or soil Ca across threshold values (x-axis). Points represent fitted slope values (i.e., the slope of the regression between the number of soil functions and the explanatory variable at each threshold), with shaded areas denoting the 95% confidence interval. A slope and its confidence interval both above zero denote a positive effect of the predictor on soil functions. Rock Ca rock calcium content, Rock Ca/Mg the ratio of rock total calcium to magnesium, Soil Ca_{ex} soil exchangeable calcium, soil Ca/Mg the ratio of soil total calcium to magnesium.

Fig. 6 | Effects of rock and soil Ca on bacterial network complexity within Ca-rich parent materials. Effects of rock Ca (total Ca content (**a**); and the ratio of total Ca to magnesium, Ca/Mg (**b**)) on soil bacterial network complexity. Effects of soil Ca (exchangeable Ca, Ca_{ex} (**c**); and Ca/Mg ratio (**d**)) on soil bacterial network complexity. Bacterial network complexity was quantified by average degree, with higher values indicating more complex networks. Solid lines represent regressions, and shaded areas denote 95% confidence intervals.

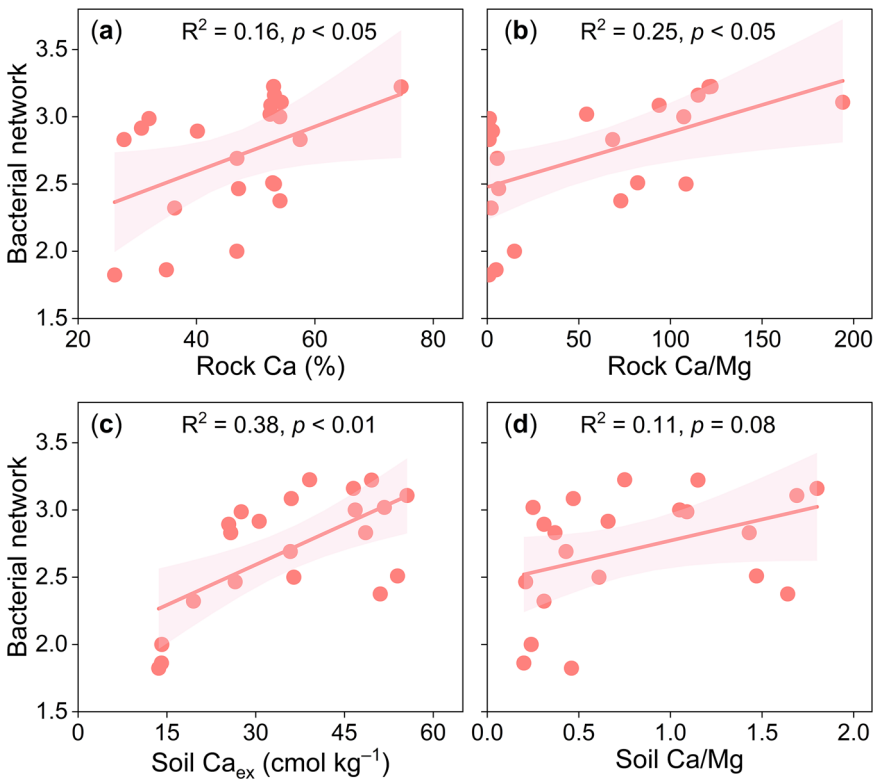

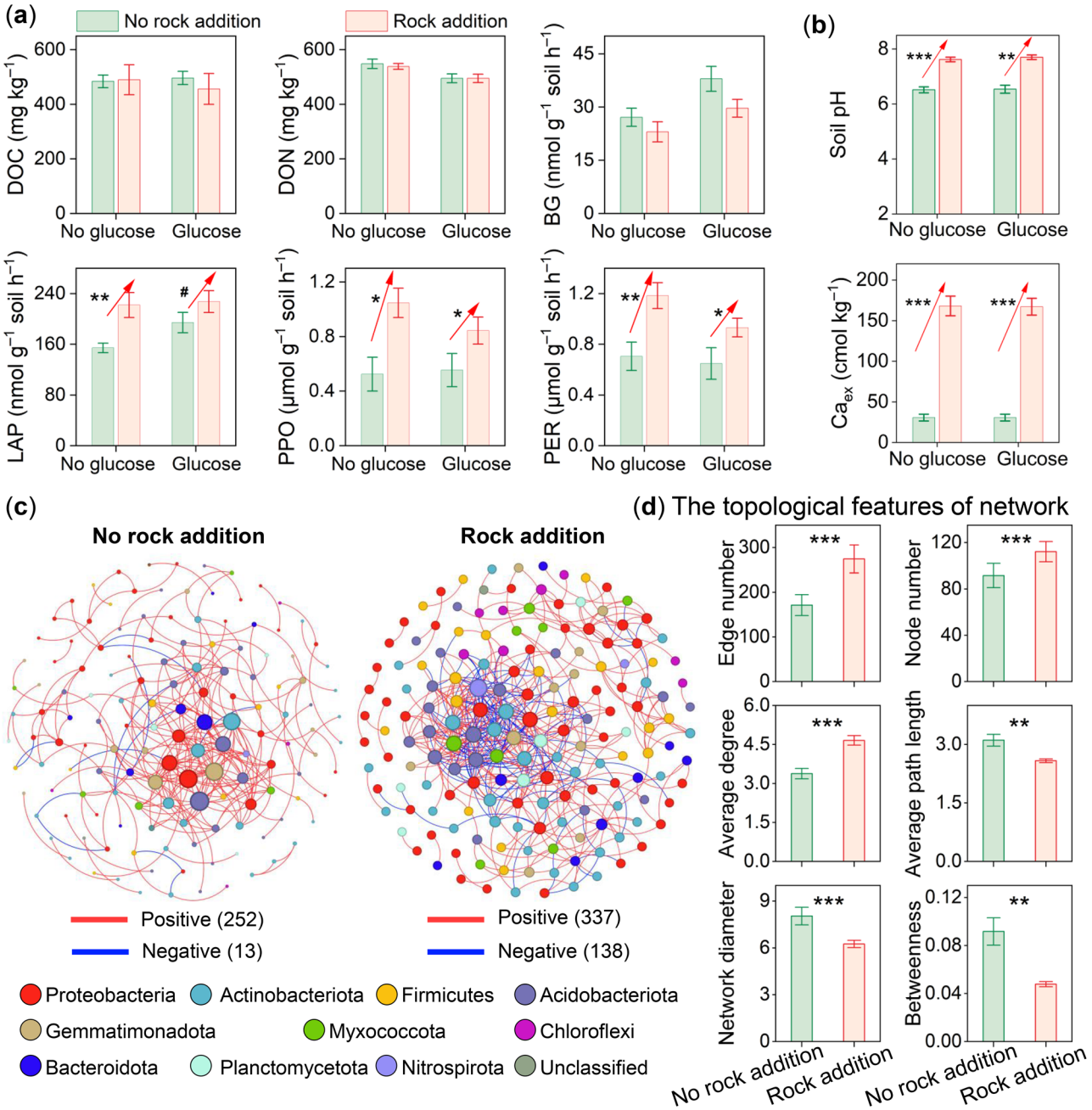

Fig. 7 | Effects of Ca-rich rock addition on carbon and nitrogen cycling and bacterial network complexity in Ca-rich soils: microcosm experiment. **a** Comparison of soil labile carbon (DOC dissolved organic carbon) and nitrogen (DON dissolved organic nitrogen), and enzyme activities linked to carbon and nitrogen cycling (BG β-D-glucosidase, LAP leucine amino peptidase, PPO polyphenol oxidase, PER peroxidase), between treatments with and without Ca-rich rock addition, under glucose-amended and unamended conditions. **b** Soil pH and exchangeable Ca (Ca_{ex}) between treatments with and without Ca-rich rock addition, under both glucose-amended and unamended conditions. **c** Co-occurrence networks of soil bacterial communities between treatments with and without Ca-rich rock addition. The sizes of the nodes (OTUs) are proportional to the number of connections. Only nodes that were significantly correlated with each other ($p < 0.05$) were connected (edges). **d** Bacterial network topological characteristics, including edge number, node number, average degree, average path length, network diameter, and betweenness, between treatments with and without Ca-rich rock addition. Higher number of edges and nodes, greater average degree, and lower average path lengths, diameters, and betweenness indicate more connected networks. Bars in (**a**), (**b**), and (**d**) represent means ± standard errors. #$p = 0.08$; *$p < 0.05$; **$p < 0.01$; ***$p < 0.001$.

network complexity not only mirrors soil resource status but also underpins the stability and persistence of critical soil functions.

Our microcosm experiment confirms that Ca-rich rock rapidly enhances soil functioning (Fig. 7a). In the short term, Ca-rich rock addition elevated the activity of oxidative enzymes critical to carbon cycling, including polyphenol oxidase and peroxidase. Notably, in the absence of external labile carbon inputs (glucose), the activities of polyphenol oxidase and peroxidase increased more markedly (Fig. 7a). This response stems primarily from carbonate dissolution, which releases Ca into the soil (Fig. 7b). The released Ca stabilizes pre-existing labile carbon within mineral-associated complexes, thereby restricting microbial access. Under these carbon-limited conditions, particularly without exogenous labile carbon supplementation, microbes increasingly depend on oxidative enzymes like polyphenol oxidase and peroxidase to decompose recalcitrant carbon[34,48]. This enzymatic shift potentially supports long-term SOC sequestration. As microbes decompose recalcitrant plant-derived carbon,

they generate microbial necromass through anabolic processes[49]. Enriched with microscopic fragments, this necromass is preferentially stabilized via Ca and mineral associations[50]. Evidence suggests that stabilization outweighs formation in driving SOC accumulation[51], though further controlled experiments are essential to substantiate this mechanism. Regarding nitrogen cycling, Ca-rich rock addition boosted leucine amino peptidase activity, likely due to elevated soil pH favoring proteolytic bacteria and the provision of Ca ion as cofactors for optimal enzyme function[34,52]. Collectively, these findings highlight that Ca-rich rock addition rapidly stimulate soil carbon and nitrogen cycling, even in systems with pre-existing high Ca levels.

Ca-rich rock addition also rapidly enhances bacterial network complexity in soils with pre-existing high Ca levels (Fig. 7c, d). Notably, Ca-rich rock addition altered soil bacterial community structure (Supplementary Fig. 8). It also increased the abundance of efficient colonizing bacterial phyla, such as Proteobacteria and Bacteroidota (Supplementary Fig. 9), with genera like *Devosia* and *Hyphomicrobium* proliferating significantly (Supplementary Fig. 10). These genera are known for their growth efficiency and contributions to critical soil functions[30]. Given the close relationship between bacterial community and soil ecosystem processes, these findings elucidate the intricate interplay among rock geochemistry, bacterial networks, and soil functioning. Practically, these findings suggests that simulating Ca-rich rock effects through methods like rock powder addition or enhanced weathering could serve as an effective strategy to manipulate microbial networks and improve soil functions, such as carbon sequestration and nutrient retention.

Our field survey showed that climate had a minor influence on soil functions and microbial network complexity. However, these effects differed between Ca-rich and Ca-poor soils (Fig. 4). In Ca-rich soils, higher temperature and precipitation elevated several extracellular enzyme activities related to carbon and nitrogen cycling (Fig. 4a). In Ca-poor soils, these factors reduce total nitrogen and phosphorus contents (Fig. 4b). Climate similarly influenced microbial network complexity in opposing ways. In Ca-rich soils, higher temperature and precipitation enhanced fungal network complexity (Supplementary Fig. 2a). In Ca-poor soils, they diminished bacterial and fungal network complexity (Supplementary Fig. 2b). These patterns suggest that parent materials modulate soil responses to climate change. For Ca-rich soils, this may stem from accelerated carbonate dissolution. Although optimal carbonate dissolution occurs at 10–15 °C[53], rising temperature coupled with precipitation boosts weathering[54]. Increased Ca release then elevates microbial activity and metabolic efficiency[30], raising enzyme activities and microbial interactions. In Ca-poor soils, higher temperature and precipitation increase microbial energy demands[55], accelerating SOM decomposition[56]. This process depletes soil nutrients and reduces microbial network complexity. Consequently, Ca-rich parent materials may sustain high soil functioning amid global climate change.

Our study establishes a framework for understanding how parent materials influence soil functioning from a bottom-up perspective. However, several limitations remain. First, although soils derived from carbonate rocks contained greater carbon, nitrogen, and phosphorus storage and supported more complex bacterial networks—correlating with rock and soil Ca—Ca alone may not explain these differences. In soils derived from clastic rocks, Ca showed no correlation with these functions, likely due to inherently low Ca levels, where minor variations have negligible impact. Further research is needed to elucidate Ca's specific role across diverse geological contexts. Second, while we attribute the strong effect of Ca-rich carbonate rocks on soil functions to their relatively rapid weathering and release of rock-derived elements, we did not directly quantify the contribution of rock weathering rates to soil functions. Third, Ca-rich bedrocks encompass various types, our study focused solely on carbonate rocks. This selective representation may introduce uncertainties; for instance, the dissolution rate of wollastonite is typically lower than that of carbonate rocks[26], potentially attenuating short-term enhancements in soil functions. Future research should encompass a broader range of Ca-rich rock types—quantifying their mineral composition and weathering kinetics—to establish a more comprehensive relationship between bedrock properties and soil functioning.

Conclusions

Our study provides observational and experimental evidence that Ca-rich parent materials promote soil carbon, nitrogen, and phosphorus storage and enhance bacterial network complexity. Additionally, complex bacterial networks are closely associated with these enhanced soil functions. These insights suggest that management strategies incorporating Ca-rich rocks could sustain or improve soil ecosystem services. By elucidating the mechanistic interplay among rock geochemistry, microbial communities, and soil functions, this research provides critical insights for enhancing soil functioning, thereby supporting human wellbeing and environmental sustainability.

Methods

Field study site description

The large-scale field survey was conducted along a southwest-to-northwest transect within Guangxi and Guizhou provinces in southwest China (latitude 22°20′–27°33′ N, longitude 104°46′–108°38′ E) (Fig. 1a). This region represents an ideal natural gradient in climate and geology, transitioning from Ca-rich to Ca-poor bedrock, providing a unique system to examine how bedrock geochemistry influences soil functions. The Ca-rich bedrock predominantly comprises carbonate rocks, including limestone, dolomite, and limestone-dolomite mixtures, forming one of the world's most extensive contiguous karst landscapes[57]. Historically, karst rocky desertification—where vegetated landscapes are degraded into bare rock due to intensive agricultural activity—was widespread in this area. However, following large-scale ecological restoration efforts, this region is now one of the areas with a fastest increase in vegetation biomass globally[58,59]. The region also features Ca-poor bedrock, primarily comprising clastic rocks (sandstone, mudstone, and conglomerate) rich in silicon and resistant to weathering due to their low soluble component content. These non-karst ecosystems are characterized by thicker soil layers, typically acidic soil pH, and higher vegetation biomass compared to the adjacent karst ecosystems, enabling a clear comparison of soil functioning across lithological contrasts.

The study region has a subtropical humid monsoonal climate, with a broad range of mean annual temperature (MAT) spanning from 12.6 °C to 21.8 °C, attributed to elevations ranging from 2233 m in the northwest to 146 m above sea level in the southwest. Mean annual precipitation (MAP) varies between 1013 and 1607 mm yr^{-1}. Climate data were sourced from the National Meteorological Information Center of China (http://data.cma.cn/). Comprehensive site-specific data, including bedrock types, climate, and dominant tree species can be found in Supplementary Table 2.

Experimental design and field sample collection

Sampling was conducted across seven areas with distinct climate in the study region. Within each area, sampling sites were established in secondary forests situated on both Ca-rich (carbonate rocks, karst ecosystems) and Ca-poor (clastic rocks, non-karst ecosystems) bedrocks (Fig. 1a). The secondary forests in each area, regardless of lithology, were ~60 ± 5 years old. Slope gradients generally ranged from 15 to 20°. Three replicate sites were selected for each bedrock type within each area. The distance between any two replicate sites within a single area exceeded 100 m but was generally less than 5 km. In some cases, to accommodate variations in lithology, forest age, and slope, the distance between sampling sites was greater. In total, 42 sampling sites were selected, with two bedrock types, seven regions, and three replicates per bedrock type.

A standardized 30 m × 30 m plot was designated at each site, where three to five slightly weathered rock samples were obtained from natural rock outcrops and pooled to represent the bedrock of the plot. In the region, carbonate rocks were extensively outcropped, allowing for rock samples to be obtained from all 21 Ca-rich bedrock sites. However, due to clastic rocks being commonly buried underground at considerable depths, only 8 out of

21 Ca-poor bedrock sites yielded rock samples. Consequently, in the subsequent analysis of factors affecting soil functions, the bedrock geochemistry was not considered for the Ca-poor bedrock sites.

Soils derived from carbonate rocks were classified as Rendzic Leptosols (Skeletic, Humic) according to the World Reference Base for Soil Resources, while soils derived from clastic rocks were classified as Acrisol or Ferralsol. Twenty mineral soil cores (0–15 cm depth, 3.8 cm diameter) were collected from each plot using a grid sampling method. Sampling points were arranged in a 4 × 5 grid with ~6 m between rows and 5 m between columns. If a designated point was obstructed (e.g., by a stone), the core was collected from the near accessible location. All cores from a plot were pooled for analysis. After removing visible roots and stones, the soil was sieved through 2 mm mesh. Fresh samples were promptly stored in iceboxes for transport and preserved at 4 °C or −80 °C upon arrival at the laboratory. Soil samples stored at 4 °C were used to analyze extracellular enzyme activity and other labile soil parameters, while those stored at −80 °C were designated to analyze microbial community structure via DNA extraction methods. The remaining soil samples underwent natural air-drying indoors and were used to assess soil physico-chemical properties.

Rock and soil properties

The outer weathering layer of each rock sample was removed using a lapidary slab saw. Subsequently, unweathered rock materials underwent a 24-h cleaning treatment with 5% hydrogen peroxide to eliminate organic matter from the rock surface[17]. The samples were then heated to 105 °C to ensure complete decomposition of the hydrogen peroxide. The rocks were crushed and milled into a fine powder, achieving a particle size of 75 μm with the aid of a grinding machine. The elemental composition of the rock, specifically Ca, Mg, and Si contents, was analyzed using an X-ray fluorescence spectrometer (Axios mAX, Malvern Panalytical B.V., Netherlands), with the final values expressed as percentages of CaO, MgO, and SiO_2, respectively.

The water holding capacity (% in mas) of undisturbed soil cores collected in steel rings was determined gravimetrically. Soil cores were saturated with deionized water for 24 h, drained under gravity for 8 h, and weighed (W_1). The cores were then oven-dried at 105 °C to constant weight (W_2), with weight of the empty steel ring recorded (W_3). Soil water holding capacity (WHC) was calculated as:

$$WHC = \frac{W_1 - W_2}{W_2 - W_3} \times 100 \quad (1)$$

SOC was quantified using acidified dichromate oxidation method (H_2SO_4–$K_2Cr_2O_7$), followed by titration with ferrous sulfate and application of an oxidation correction factor. Dissolved organic carbon was extracted with 0.5 M K_2SO_4 and quantified using a total organic carbon analyzer (TOC-Vwp; Shimadzu, Japan). Microbial biomass carbon was assessed using the chloroform fumigation-extraction method[60]. Total nitrogen content was measured with an elemental analyzer (vario MAX cube, Elementar, Hanau, Germany). Ammonium and nitrate were extracted using 2 M KCl and quantified via continuous flow analyzer (AutoAnalyzer 3; SEAL Analytic, Germany), with total inorganic nitrogen calculated as their sum. Total phosphorus was quantified via an ultraviolet spectrophotometer through the molybdenum antimony blue colorimetry method. Prior to analysis, soil samples underwent alkali fusion to convert inherent phosphorus into a soluble form suitable for detection[61]. Mineral-associated organic carbon was analyzed using a physical fractionation method, in which soil was separated into the mineral-associated organic matter fraction[62]. The organic carbon content of this fraction was then measured. Detailed procedures are provided in Supplementary Method 1.

Soil pH was determined in a 1:2.5 soil-to-water suspension using a pH meter (FE20K; Mettler-Toledo, Greifensee, Switzerland). Exchangeable Ca and Mg were extracted using 1 mol L^{-1} ammonium acetate. Free iron (hydr) oxides, representing pedogenic iron, were extracted using the citrate-bicarbonate-dithionite method, while amorphous iron (hydr)oxides, indicative of short-range order iron phases, were extracted using an ammonium oxalate buffer[63]. The contents of exchangeable Ca and Mg, as well as free iron (hydr)oxides and amorphous Fe (hydr)oxides were determined using an inductively coupled plasma emission spectrometer (5110 ICP-OES; Agilent, Santa Clara, CA, USA). Soil $CaCO_3$ was determined by acid–base titration. Specifically, 3.0–10.0 g of air-dried soil, sieved to 100 mesh and containing ~0.2–0.4 g of $CaCO_3$ (verified by a semi-quantitative HCl test), was dissolved in 20 mL of 0.5 mol L^{-1} HCl. The excess acid was then back-titrated with 0.25 mol L^{-1} NaOH, and the volume of NaOH consumed was recorded to calculate the equivalent $CaCO_3$ content. Soil total Ca and Mg contents were determined using the same method as for rock samples, with final values expressed as percentages of CaO and MgO.

Soil extracellular enzyme activities and microbial carbon use efficiency

The extracellular enzyme activities involved in the carbon cycle (α-glucosidase, β-D-glucosidase, β-xylosidase, and β-D-cellobiosidase), nitrogen cycle (leucine amino peptidase and β-N-acetyl-glucosaminidase), and phosphorus cycle (acid or alkaline phosphatase) were measured using microplate protocols[64]. Briefly, the soil samples were homogenized in sodium acetate buffer (50 mM) at pH 5.0, and the assays were performed using 96-well black microplates. The absolute enzyme activity (nmol g^{-1} h^{-1} dry soil) was calculated after accounting for blanks, negative controls, and quenching.

Microbial carbon use efficiency, defined as the proportion of assimilated carbon retained in microbial biomass, serves as an integrative metric for understanding microbial regulation of SOC loss and accumulation[65]. Microbial carbon use efficiency was quantified using a substrate-independent approach that measures the incorporation of ^{18}O-H_2O into microbial DNA[66]. Further details can be found in Supplementary Method 2.

DNA extraction and high-throughput sequencing

Soil DNA was extracted from 0.5 g of freeze-dried soil using the FastDNA Spin Kit (MP Biomedicals, Santa Ana, CA, USA). The DNA quantity and quality were assessed using a NanoDrop 2000 UV-VIS spectrophotometer (Thermo Fisher Scientific, Wilmington, DE, USA). The abundance of bacterial 16S rRNA and fungal ITS genes was quantified using a 9600 Plus quantitative PCR system (Bioer Technology, Hangzhou, China). Amplifications were carried out with the primer pairs 341F (CCTAYGGGRBGCASCAG)/806R (GGACTACHVGGGTWTCTAAT) for bacterial 16S rRNA genes, and ITS1F (CTTGGTCATTTAGAGGAAGTAA)/ITS2R (GCTGCGTTCTTCATCGATGC) for fungal ITS genes. The 20 μL PCR reaction mixture included 10 μL of 2× ChamQ SYBR Color qPCR Master Mix, 0.4 μL of each primer (5 μM), 2 μL of DNA template, and sterile ddH_2O. The PCR protocol was as follows: initial denaturation at 95 °C for 5 min, followed by 40 cycles of 95 °C for 30 s, 56 °C for 30 s, and 72 °C for 40 s.

Bacterial and fungal community structure were further analyzed via 16S and ITS gene amplicon sequencing, respectively. For bacterial 16S rRNA gene sequences, the primer pair 338F (5′-ACTCCTACGGGAGGCAGCAG-3′) and 806R (5′-GGACTACHVGGGTWTCTAAT-3′) was used. For fungal ITS gene sequences, the primer pair ITS1F (5′-CTTGGTCATTTAGAGGAAGTAA-3′) and ITS2R (5′-GCTGCGTTCTTCATCGATGC-3′) was employed. Purified PCR products were sequenced on the Illumina MiSeq PE300 platform (Illumina, San Diego, CA, USA). Sequencing data were processed using QIIME 2, with raw reads denoised using the q2-dada2-plugin. Unique sequences were clustered into operational taxonomic units (OTUs) at 97% identity using the q2-vsearch plugin. Taxonomic assignment for bacterial and fungal OTUs was performed using the SILVA_v132 and UNITE_v8.3 reference databases, respectively. Microbial α-diversity, including the Shannon-Wiener index, was computed using the "RAM" package in R (R Core Team, Vienna, Austria).

Microcosm experiment

To complement the large-scale field survey, we conducted a microcosm experiment to further investigate the effect of Ca-rich rock on soil carbon

and nitrogen cycling and bacterial network complexity in soils with high Ca content. Soil samples were collected from three distinct locations within the karst region of southwest China, each representing a unique climate regime and differing from the field study sites. Comprehensive data on the sampling sites, including coordinates, elevation, and climate, are provided in Supplementary Table 3. Soils were derived from carbonate-rich parent materials and classified as Rendzic Leptosols (Skeletic, Humic) according to the World Reference Base for Soil Resources. Soil samples were collected from the 0–10 cm mineral layer after removing any litter layer. Roots and stones were carefully removed, and the soil was sieved through a 2 mm mesh for homogenization. The sieved samples were then transported to the laboratory for the microcosm experiment.

The experiment included treatments with and without Ca-rich rock powder added to soil samples, alongside treatments with and without exogenous labile carbon (glucose; Fig. 1b). The inclusion of carbon addition treatments was designed to assess whether the effects of Ca-rich rock on soil carbon and nitrogen cycling remain consistent under conditions with or without exogenous labile carbon. Each treatment was replicated three times, resulting in a total of 36 experimental microcosms. The Ca-rich rock used in the experiment was derived from unweathered limestone, which was crushed to pass through a 2 mm mesh size to promote rapid weathering and dissolution during incubation. For control treatments without Ca-rich rock addition, quartz sand of comparable weight and particle size was used to ensure consistency across treatments. Both the limestone and quartz sand samples were sterilized using two times a dose of gamma radiation (50 kGy each) to eliminate microbial contamination.

Initially, 40 g of soil from each treatment was preincubated in a 250 mL bottle in darkness at 25 °C for 7 days, with soil moisture maintained at 55% of its water holding capacity. Following pre-incubation, three replicates from each treatment received 4 g of limestone powder, while the remaining three replicates received an equivalent amount of quartz sand powder. For treatments involving exogenous carbon addition, 1 mL of a glucose solution (40 mg mL^{-1} carbon content) was added to provide a readily available carbon source for soil microbes. For treatments without exogenous carbon addition, an equal volume of deionized water was added. Soil microcosms were then incubated at 25 °C for 64 days, with the soil moisture kept at 55% water holding capacity throughout the incubation period.

At the end of the incubation, soil samples were collected to measure dissolved organic carbon, dissolved organic nitrogen, and extracellular enzyme activities. The activities of hydrolytic enzymes, including β-D-glucosidase and leucine amino peptidase, as well as oxidative enzymes, such as polyphenol oxidase and peroxidase, were determined. Methods for determining dissolved organic carbon, β-D-glucosidase, and leucine amino peptidase aligned with those used in the field study. Dissolved organic nitrogen was calculated by subtracting inorganic nitrogen (ammonium and nitrate) from total dissolved nitrogen. Concentrations of ammonium and nitrate were determined following the same methods as in the field study. Total dissolved nitrogen was extracted using 0.5 M potassium sulfate and determined with a dissolved organic carbon/total nitrogen analyzer (TOC-VCPH, Shimadzu Corporation, Japan). For oxidative enzymes, L-3,4-dihydroxyphenylalanine was added to each microtiter plate well containing soil suspension, and half of the wells received an additional H_2O_2 solution for peroxidase measurement. Plates were incubated in darkness at 25 °C for up to 18 h. The bacterial community structure in the microcosm soils was analyzed using 16S gene amplicon sequencing, following the same primer pair and methodology as employed in the field study.

Assessment of soil functions

For the field study, we evaluated soil functions using 14 parameters organized into four functional groups: (1) water retention, indicated by water holding capacity; (2) carbon cycling, reflected by SOC, microbial biomass carbon, dissolved organic carbon, and extracellular enzyme activities including α-glucosidase, β-D-glucosidase, β-xylosidase, and β-D-cellobiosidase; (3) nitrogen cycling, indicated by total nitrogen, total inorganic nitrogen, and enzyme activities β-N-acetyl-glucosaminidase and leucine amino peptidase; and (4) phosphorus cycling, reflected by total phosphorus and enzyme activity phosphatas. These parameters encompass stocks of matter and energy, capturing both slow abiotic and biotic processes as well as short-term biotic process rates[67]. They provide comprehensive insights into critical soil functions, including water retention, carbon cycling, nitrogen cycling, and phosphorus cycling[21,68].

For the microcosm experiment, we evaluated soil functions using six parameters organized into two groups: (1) carbon cycling, reflected by dissolved organic carbon and the activities of extracellular enzymes, including β-D-glucosidase and oxidative enzymes (polyphenol oxidase and peroxidase), and (2) nitrogen cycling, indicated by dissolved organic nitrogen and leucine amino peptidase activity. These parameters were chosen to represent labile soil carbon and nitrogen fractions, along with enzymatic process rates, as they are responsive to short-term changes and provide insights into soil carbon and nitrogen cycling within the experimental timeframe.

Soil functions in the field study was assessed using two approaches: the single-function approach and threshold approach. The single-function approach provides direct insights into individual functions. The threshold approach was used to quantify soil functioning by determining the number of soil functions surpassing a defined threshold relative to the maximum observed value of each function[69]. This approach evaluates the extent to which multiple functions are operating at high levels concurrently. The maximum level for each function was defined as the average of the top four measured values. We applied continuous multiple thresholds (ranging from 5% to 99%, in 1% intervals) to calculate how many soil functions reached each threshold (i.e. the percentage of the function's maximum). The threshold approach and associated figure generation were implemented using the "multifunc" package in R[69].

Co-occurrence networks of soil microbial communities

Co-occurrence networks of microbial communities for both the field study and the microcosm experiment were constructed using the WGCNA package based on Spearman's correlation matrices[70]. For these analyses, only OTUs with relative abundance greater than 0.01% and present in at least 50% of the total samples were included. In these networks, OTUs are represented as nodes, while correlations between OTUs are depicted as edges. Random matrix theory was applied to identify appropriate thresholds[71]. The Benjamini-Hochberg false discovery rate method was used to adjust the p values for the correlations. Only correlations with an adjusted p value less than 0.05 and a score exceeding the threshold (Supplementary Table 4) were included. Network visualization was performed using Gephi 0.9.2 (Gephi, Bordeaux, France). The topological characteristics of each sample's networks were analyzed using subgraph function via the "igraph" package in R[72]. Key parameters describing network topological characteristics included edge number (connections among nodes), node number (the number of OTUs), average degree (average number of connections per node), average path length (average distance between all pairs of nodes), network diameter (maximum distance between nodes), and betweenness (frequency of a node acting as a bridge along the shortest path between two other nodes). A higher number of edges and nodes, greater average degree, and lower average path lengths, diameters, and betweenness indicate a more connected network, suggesting increased complexity of microbial networks[25].

Statistical analyses

The experimental data were first tested for normality and homogeneity of variance. Where necessary, natural log transformations were applied to meet these criteria. The effects of parent material type (Ca-rich vs. Ca-poor) on soil properties, functions, microbial characteristics, and plant biomass carbon (method described in Supplementary Method 3) in the field experiment were assessed using independent samples t-tests. The effect of rock addition on these variables in the microcosm experiment was assessed using paired t-tests.

Next, random forest analysis was employed to quantify the effects of climate, rock geochemistry, soil pH and minerals, and microbial properties on each soil function and microbial network complexity for the field study. Predictor importance was assessed using the permutation-based increase in mean squared error (%IncMSE) over 100 permutations of the response variable, and variables with $p < 0.05$ were deemed significant. Pearson's correlation analysis was then applied to discern whether these factors exerted a positive or negative correlation with the response variables. These analyses and associated figure generation were performed in R using the "randomForest", "corrr", and "ggplot2" packages.

Finally, ordinary least-squares regression was used to explore the relationships between multiple-threshold functions and the significant predictors identified by the random forest analysis. This approach was also used to investigate the associations between microbial network complexity and rock and soil Ca (including Ca content and the Ca/Mg ratio), alongside other dependent and independent variables. Because causal direction between microbial network complexity and soil functions cannot be inferred from our design, we assessed their association using Pearson's correlation only. Unless otherwise specified, all other figures were generated using Origin 2025 (OriginLab Corporation, Northampton, MA, USA).

Reporting summary

Further information on research design is available in the Nature Portfolio Reporting Summary linked to this article.

Data availability

Raw sequence data have been deposited in the National Center for Biotechnology Information (NCBI) Sequence Read Archive under BioProject accession number PRJNA1308311. Additional datasets generated and analyzed during the current study are openly available in "Zenodo" at https://doi.org/10.5281/zenodo.14037755.

Received: 18 March 2025; Accepted: 2 September 2025;
Published online: 08 October 2025

References

1. Bardgett, R. D. & van der Putten, W. H. Belowground biodiversity and ecosystem functioning. *Nature* **515**, 505–511 (2014).
2. Griscom, B. W. et al. Natural climate solutions. *Proc. Natl. Acad. Sci.* **114**, 11645–11650 (2017).
3. Kuzyakov, Y. & Zamanian, K. Reviews and syntheses: Agropedogenesis - humankind as the sixth soil-forming factor and attractors of agricultural soil degradation. *Biogeosciences* **16**, 4783–4803 (2019).
4. Yuan, Z. et al. Divergent above- and below-ground biodiversity pathways mediate disturbance impacts on temperate forest multifunctionality. *Glob. Change Biol.* **27**, 2883–2894 (2021).
5. Maestre, F. T. et al. Plant species richness and ecosystem multifunctionality in global drylands. *Science* **335**, 214–218 (2012).
6. Chen, S. et al. Freeze-thaw strength increases microbial stability to enhance diversity-soil multifunctionality relationship. *Commun. Earth Environ.* **5**, 578 (2024).
7. Fang, Q. et al. Mineral weathering is linked to microbial priming in the critical zone. *Nat. Commun.* **14**, 345 (2023).
8. Hemingway, J. D. et al. Mineral protection regulates long-term global preservation of natural organic carbon. *Nature* **570**, 228–231 (2019).
9. Slessarev, E. W., Chadwick, O. A., Sokol, N. W., Nuccio, E. E. & Pett-Ridge, J. Rock weathering controls the potential for soil carbon storage at a continental scale. *Biogeochemistry* **157**, 1–13 (2022).
10. Rowley, M. C., Grand, S., Adatte, T. & Verrecchia, E. P. A cascading influence of calcium carbonate on the biogeochemistry and pedogenic trajectories of subalpine soils, Switzerland. *Geoderma* **361**, 12 (2020).
11. Augusto, L., Achat, D. L., Jonard, M., Vidal, D. & Ringeval, B. Soil parent material—A major driver of plant nutrient limitations in terrestrial ecosystems. *Glob. Change Biol.* **23**, 3808–3824 (2017).
12. Hartmann, J., Moosdorf, N., Lauerwald, R., Hinderer, M. & West, A. J. Global chemical weathering and associated P-release — The role of lithology, temperature and soil properties. *Chem. Geol.* **363**, 145–163 (2014).
13. Houlton, B. Z., Morford, S. L. & Dahlgren, R. A. Convergent evidence for widespread rock nitrogen sources in Earth's surface environment. *Science* **360**, 58 (2018).
14. He, X. et al. Parental material and climate jointly determine the biomass and diversity of soil microbial communities along an elevational gradient on a subtropical karst mountain. *J. Biogeogr.* **51**, 1185–1198 (2024).
15. Li, Y.-Z. et al. Toward soil carbon storage: The influence of parent material and vegetation on profile-scale microbial community structure and necromass accumulation. *Soil Biol. Biochem.* **193**, 109399 (2024).
16. Landeweert, R., Hoffland, E., Finlay, R. D., Kuyper, T. W. & van Breemen, N. Linking plants to rocks: ectomycorrhizal fungi mobilize nutrients from minerals. *Trends Ecol. Evol.***16**, 248–254 (2001).
17. Dynarski, K. A., Morford, S. L., Mitchell, S. A. & Houlton, B. Z. Bedrock nitrogen weathering stimulates biological nitrogen fixation. *Ecology* **100**, e02741 (2019).
18. Xiao, D. et al. Comparison of bacterial and fungal diversity and network connectivity in karst and non-karst forests in southwest China. *Sci. Total Environ.* **822**, 153179 (2022).
19. Sokol, N. W. et al. Life and death in the soil microbiome: how ecological processes influence biogeochemistry. *Nat. Rev. Microbiol.* **20**, 415–430 (2022).
20. Barberán, A., Bates, S. T., Casamayor, E. O. & Fierer, N. Using network analysis to explore co-occurrence patterns in soil microbial communities. *ISME J.* **6**, 343–351 (2011).
21. Delgado-Baquerizo, M. et al. Multiple elements of soil biodiversity drive ecosystem functions across biomes. *Nat. Ecol. Evol.***4**, 210–220 (2020).
22. Wagg, C., Schlaeppi, K., Banerjee, S., Kuramae, E. E. & van der Heijden, M. G. A. Fungal-bacterial diversity and microbiome complexity predict ecosystem functioning. *Nat. Commun.* **10**, 4841 (2019).
23. Yuan, M. M. et al. Climate warming enhances microbial network complexity and stability. *Nat. Clim. Change* **11**, 343–U100 (2021).
24. Durán, P. et al. Microbial interkingdom interactions in roots promote Arabidopsis survival. *Cell* **175**, 973–983. e914 (2018).
25. Jiao, S., Lu, Y. H. & Wei, G. H. Soil multitrophic network complexity enhances the link between biodiversity and multifunctionality in agricultural systems. *Glob. Change Biol.* **28**, 140–153 (2022).
26. Liu, Z. H., Dreybrodt, W. & Liu, H. Atmospheric CO_2 sink: silicate weathering or carbonate weathering?. *Appl. Geochem.* **26**, S292–S294 (2011).
27. Sridhar, B. et al. Microbial community shifts correspond with suppression of decomposition 25 years after liming of acidic forest soils. *Glob. Change Biol.* **28**, 5399–5415 (2022).
28. Tang, Y. et al. Higher free-living N2 fixation at rock-soil interfaces than topsoils during vegetation recovery in karst soils. *Soil Biol. Biochem.* **159**, 108286 (2021).
29. Geng, Y. et al. Phosphorus biogeochemistry regulated by carbonates in soil. *Environ. Res.* **214**, 113894 (2022).
30. Shabtai, I. A. et al. Calcium promotes persistent soil organic matter by altering microbial transformation of plant litter. *Nat. Commun.* **14**, 6609 (2023).
31. Rowley, M. C., Grand, S. & Verrecchia, ÉP. Calcium-mediated stabilisation of soil organic carbon. *Biogeochemistry* **137**, 27–49 (2018).

32. Hu, P. et al. Lithological controls on soil aggregates and minerals regulate microbial carbon use efficiency and necromass stability. *Environ. Sci. Technol.* **58**, 21186–21199 (2024).
33. Yang, T. et al. Greater variation of soil organic carbon in limestone- than shale-based soil along soil depth in a subtropical coniferous forest within a karst faulted basin of China. *Catena* **246**, 108389 (2024).
34. Sinsabaugh, R. L. et al. Stoichiometry of soil enzyme activity at global scale. *Ecol. Lett.* **11**, 1252–1264 (2008).
35. Holloway, J. M. & Dahlgren, R. A. Nitrogen in rock: occurrences and biogeochemical implications. *Glob. Biogeochem. Cycles* **16**, 65-61–65-17 (2002).
36. von Wandruszka, R. Phosphorus retention in calcareous soils and the effect of organic matter on its mobility. *Geochem. Trans.* **7**, 6 (2006).
37. Dick, W. A., Cheng, L. & Wang, P. Soil acid and alkaline phosphatase activity as pH adjustment indicators. *Soil Biol. Biochem.* **32**, 1915–1919 (2000).
38. Anikwe, M. A. N., Eze, J. C. & Ibudialo, A. N. Influence of lime and gypsum application on soil properties and yield of cassava (Manihot esculenta Crantz.) in a degraded Ultisol in Agbani, Enugu Southeastern Nigeria. *Soil Tillage Res.* **158**, 32–38 (2016).
39. Liu, X., Feng, T., Zhang, Y., Liu, Y. & Wang, P. Vegetation restoration affects soil hydrological processes in typical natural and planted forests on the Loess Plateau. *J. Hydrol.* **650**, 132465 (2025).
40. Qiu, L. et al. Erosion reduces soil microbial diversity, network complexity and multifunctionality. *ISME J.* **15**, 2474–2489 (2021).
41. Dominguez, D. C. Calcium signalling in bacteria. *Mol. Microbiol.* **54**, 291–297 (2004).
42. Dong, H. et al. A critical review of mineral–microbe interaction and co-evolution: mechanisms and applications. *Natl. Sci. Rev.* **9**, https://doi.org/10.1093/nsr/nwac128 (2022).
43. Dou, X. et al. Calcium forms influence soil organic carbon by mediating labile organic carbon fractions, carbon pool management indices and microbial communities in calcareous alkaline soils. *Plant Soil* https://doi.org/10.1007/s11104-024-07115-6 (2024).
44. Rousk, J. et al. Soil bacterial and fungal communities across a pH gradient in an arable soil. *ISME J.* **4**, 1340–1351 (2010).
45. Morriën, E. et al. Soil networks become more connected and take up more carbon as nature restoration progresses. *Nat. Commun.* **8**, 14349 (2017).
46. Luo, S. et al. Grassland degradation-induced declines in soil fungal complexity reduce fungal community stability and ecosystem multifunctionality. *Soil Biol. Biochem.* **176**, 108865 (2023).
47. Zhang, C. et al. Simplified microbial network reduced microbial structure stability and soil functionality in alpine grassland along a natural aridity gradient. *Soil Biol. Biochem.* **191**, 109366 (2024).
48. Burns, R. G. et al. Soil enzymes in a changing environment: current knowledge and future directions. *Soil Biol. Biochem.* **58**, 216–234 (2013).
49. Liang, C., Schimel, J. P. & Jastrow, J. D. The importance of anabolism in microbial control over soil carbon storage. *Nat. Microbiol.* **2**, 1–6 (2017).
50. Klink, S. et al. Stable isotopes reveal that fungal residues contribute more to mineral-associated organic matter pools than plant residues. *Soil Biol. Biochem.* **168**, 108634 (2022).
51. Xiao, K.-Q. et al. Beyond microbial carbon use efficiency. *Natl. Sci. Rev.* **11**, https://doi.org/10.1093/nsr/nwae059 (2024).
52. Strynadka, N. C. J. & James, M. N. G. Towards an understanding of the effects of calcium on protein structure and function. *Curr. Opin. Struct. Biol.* **1**, 905–914 (1991).
53. Gaillardet, J., Calmels, D., Romero-Mujalli, G., Zakharova, E. & Hartmann, J. Global climate control on carbonate weathering intensity. *Chem. Geol.* **527**, 118762 (2019).
54. Zeng, S., Liu, Z. & Kaufmann, G. Sensitivity of the global carbonate weathering carbon-sink flux to climate and land-use changes. *Nat. Commun.* **10**, 5749 (2019).
55. Dijkstra, P. et al. Effect of temperature on metabolic activity of intact microbial communities: Evidence for altered metabolic pathway activity but not for increased maintenance respiration and reduced carbon use efficiency. *Soil Biol. Biochem.* **43**, 2023–2031 (2011).
56. Zhao, X., Yang, Y., Shen, H., Geng, X. & Fang, J. Global soil-climate-biome diagram: linking surface soil properties to climate and biota. *Biogeosciences* **16**, 2857–2871 (2019).
57. Wang, K. et al. Karst landscapes of China: patterns, ecosystem processes and services. *Landsc. Ecol.* **34**, 2743–2763 (2019).
58. Chen, C. et al. China and India lead in greening of the world through land-use management. *Nat. Sustain.***2**, 122–129 (2019).
59. Tong, X. et al. Reforestation policies around 2000 in southern China led to forest densification and expansion in the 2010s. *Commun. Earth Environ.* **4**, 260 (2023).
60. Wu, J., Joergensen, R. G., Pommerening, B., Chaussod, R. & Brookes, P. C. Measurement of soil microbial biomass c by fumigation extraction - an automated procedure. *Soil Biol. Biochem.* **22**, 1167–1169 (1990).
61. Syers, J. K., Williams, J. D. H. & Walker, T. W. The determination of total phosphorus in soils and parent materials. *N.Z. J. Agric. Res.* **11**, 757–762 (1968).
62. Cotrufo, M. F., Ranalli, M. G., Haddix, M. L., Six, J. & Lugato, E. Soil carbon storage informed by particulate and mineral-associated organic matter. *Nat. Geosci.* **12**, 989 (2019).
63. Chen, L. et al. Soil carbon persistence governed by plant input and mineral protection at regional and global scales. *Ecol. Lett.* **24**, 1018–1028 (2021).
64. Saiya-Cork, K. R., Sinsabaugh, R. L. & Zak, D. R. The effects of long term nitrogen deposition on extracellular enzyme activity in an Acer saccharum forest soil. *Soil Biol. Biochem.* **34**, 1309–1315 (2002).
65. Tao, F. et al. Microbial carbon use efficiency promotes global soil carbon storage. *Nature* https://doi.org/10.1038/s41586-023-06042-3 (2023).
66. Spohn, M., Klaus, K., Wanek, W. & Richter, A. Microbial carbon use efficiency and biomass turnover times depending on soil depth – Implications for carbon cycling. *Soil Biol. Biochem.* **96**, 74–81 (2016).
67. Garland, G. et al. A closer look at the functions behind ecosystem multifunctionality: a review. *J. Ecol.* **109**, 600–613 (2021).
68. Hu, W. et al. Aridity-driven shift in biodiversity–soil multifunctionality relationships. *Nat. Commun.* **12**, 5350 (2021).
69. Byrnes, J. E. K. et al. Investigating the relationship between biodiversity and ecosystem multifunctionality: challenges and solutions. *Methods Ecol. Evol.***5**, 111–124 (2014).
70. Langfelder, P. & Horvath, S. WGCNA: an R package for weighted correlation network analysis. *BMC Bioinforma.* **9**, 559 (2008).
71. Luo, F., Zhong, J. X., Yang, Y. F., Scheuermann, R. H. & Zhou, J. Z. Application of random matrix theory to biological networks. *Phys. Lett. A* **357**, 420–423 (2006).
72. Ma, B. et al. Geographic patterns of co-occurrence network topological features for soil microbiota at continental scale in eastern China. *ISME J.* **10**, 1891–1901 (2016).

Acknowledgements

This study was supported by the Funds for International Cooperation and Exchange of the National Natural Science Foundation of China [42361144886], the Joint Funds of the National Natural Science Foundation of China [U23A20155], the Guangxi Key Research and Development Program [AB24010076], and the National Natural Science Foundation of China [42377351]. We thank the Institutional Center for Shared Technologies and Facilities of Institute of Subtropical Agriculture, CAS, for supporting the analyses of rock and soil properties.

Author contributions

P. H.: conceptualization, investigation, methodology, data curation, visualization, writing—original draft, writing—review & editing. W. Z.:

conceptualization, funding acquisition, supervision, writing—review & editing. W. W.: writing—review & editing. J. C.: writing—review & editing. D. A.: writing—review & editing. J. Z.: methodology, investigation. D. X.: investigation. X. H.: investigation. J. L.: investigation. H. C.: methodology. J. X.: investigation. X. L.: investigation. T. T.: investigation. H. W.: visualization. K. W.: conceptualization, funding acquisition, supervision, writing—review & editing.

Competing interests
The authors declare no competing interests.

Additional information
Supplementary information The online version contains supplementary material available at https://doi.org/10.1038/s43247-025-02761-9.

Correspondence and requests for materials should be addressed to Wei Zhang or Kelin Wang.

Peer review information *Communications Earth and Environment* thanks Andre Eger, Jennifer Pensky and the other, anonymous, reviewer(s) for their contribution to the peer review of this work. Peer review was single-anonymous OR Peer review was double-anonymous.

Reprints and permissions information is available at http://www.nature.com/reprints

Publisher's note Springer Nature remains neutral with regard to jurisdictional claims in published maps and institutional affiliations.

Open Access This article is licensed under a Creative Commons Attribution-NonCommercial-NoDerivatives 4.0 International License, which permits any non-commercial use, sharing, distribution and reproduction in any medium or format, as long as you give appropriate credit to the original author(s) and the source, provide a link to the Creative Commons licence, and indicate if you modified the licensed material. You do not have permission under this licence to share adapted material derived from this article or parts of it. The images or other third party material in this article are included in the article's Creative Commons licence, unless indicated otherwise in a credit line to the material. If material is not included in the article's Creative Commons licence and your intended use is not permitted by statutory regulation or exceeds the permitted use, you will need to obtain permission directly from the copyright holder. To view a copy of this licence, visit http://creativecommons.org/licenses/by-nc-nd/4.0/.

© The Author(s) 2025